Periodically Pulsed Spin Dynamics: Scaling Behavior of Semiclassical Wave Functions

K. Nakamura
Fukuoka Institute of Technology, Higashi-ku, Fukuoka 811-02, Japan
Y. Okazaki[a]
Department of Physics, Kyoto University, Kyoto 606, Japan
and
A. R. Bishop
Theoretical Division and Center for Nonlinear Studies, Los Alamos National Laboratory, Los Alamos, New Mexico 87545
(Received 28 April (1986)

Quantum analogs of Kolmogorov-Arnol'd-Moser tori and chaos in a periodically pulsed single-spin system are studied in the semiclassical regime. Wave functions (quasienergy states) are described in a spin-coherent state representation. Their projected binary-phase patterns are characterized in terms of the fractal dimensions of their perimeters.

PACS numbers: 05.45.+b, 03.65.-w, 75.10.Jm

Quantum analogs of classical chaos in driven nonautonomous systems have received growing theoretical and experimental attention. In particular, much effort has been concentrated on the study of a quantum kicked rotator[1] which corresponds to the standard map in the classical limit. Analyses of wave functions and associated contours[2] show that full development of fine structure (e.g., tendrils) on all scales is suppressed because of the finiteness of $\hbar$—distinguishing the situation from, e.g., diffusion processes in classical fluid dynamics. This fact, however, suggests at the same time the possibility of finding tendrils with much finer structures, i.e., "fractal" tendrils, if $\hbar$ is decreased.

Chaos in driven spin systems has recently become realized and its study constitutes a very active research field,[3] though experiments to date have been limited to dissipative spin-wave dynamics. Fully nonlinear dynamics for noninteracting spins, both classical and quantum, is also an attractive candidate by which to study classical chaos and its quantum counterpart. The advantage of spin systems is that, as a result of the finite-dimensional Hilbert space, we can readily tune the value of $\hbar$ without artificial truncation procedures in quantum-mechanical treatments.

In this Letter, we consider wave functions (quasienergy eigenstates[1]) for a periodically kicked spin system and demonstrate their "quasifractal" structures in semiclassically large-spin regions. Let us consider the single-spin Hamiltonian, common to both classical and quantum spin variables $\mathbf{S}$,

$$H = A(S_z)^2 - \mu B S_x \sum_{n=-\infty}^{\infty} \delta(t - 2\pi n), \tag{1}$$

where A (>0) and B (>0) are an easy-plane anisotropy and magnetic field along the x axis, respectively. Some aspects of the quantum dynamics for the same systems, Eq. (1), were recently independently studied by two groups,[4] but without any systematic discussion of wave-function structure.

Before proceeding to the quantum-mechanical treatment, we shall present brief results for classical dynamics. Then $\mathbf{S}$ is a three-component vector $\mathbf{S} = S_x\mathbf{e}_x + S_y\mathbf{e}_y + S_z\mathbf{e}_z$ ($\mathbf{e}$ is a unit vector), which obeys the equation of motion

$$d\mathbf{S}/dt = \mathbf{S} \times (-\delta H/\delta \mathbf{S}) = \mathbf{S}x\left[-2AS_z\mathbf{e}_z + \mu B\mathbf{e}_x \sum_{n=-\infty}^{\infty} \delta(t - 2\pi n)\right]. \tag{2}$$

The magnitude $\mathbf{S}^2$ is conserved in Eq. (2), and is now normalized to unity. $\mathbf{S}$ is then described in polar coordinates, i.e., $\mathbf{S} = (S_x, S_y, S_z) = (\sin\theta\cos\phi, \sin\theta\sin\phi, \cos\theta)$. The discrete map can be constructed for successive values $\{\mathbf{S}_n\}$, where $\mathbf{S}_n$ is the value of $\mathbf{S}$ at $t = 2\pi n + 0$, i.e., just after the nth pulse. In the interval $2\pi n + 0 \leq t \leq 2\pi(n+1) - 0$, the magnetic field is not operative in Eq. (2) and thus $\mathbf{S}_n$ is transformed into $\Gamma = R_z(\alpha)\mathbf{S}_n$ at $t = 2\pi(n+1) - 0$, where the operator $R_z(\alpha)$ denotes a rotation by angle $\alpha = 4\pi AS_{nz}$ around the z axis. Then, the $(n+1)$th pulse during $2\pi(n+1) - 0 \leq t \leq 2\pi(n+1) + 0$ rotates Γ by angle $\beta = -\mu B$ around the x axis, yielding $\mathbf{S}_{n+1} = R_x(\beta)\Gamma$.

Eventually, the combined map $\mathbf{S}_{n+1} = R_x(\beta)R_z(\alpha)\mathbf{S}_n$ is obtained, which we have solved with $A = 1.0$ and $0.0 \leq \mu B \leq 1.0$.[5] The results are given in polar coordinates in Figs. 1(a)–1(c). We see that Kolmogorov-Arnol'd-Moser (KAM) tori, which dominate in weak magnetic field regions, begin to collapse with increasing field. Investigation of our extensive data as a function of μB indicates the presence of two characteristic fields $\mu B_1 \cong 0.1$ and $\mu B_2 \cong 0.5$, where the fraction of chaotic trajectories increases strongly and the last KAM torus[5] disappears, respectively.

The corresponding quantum dynamics is governed

by the time-dependent Schrödinger equation for a wave function ψ: $i\hbar\, d\psi/dt = H\psi$ with H being the quantum version of Eq. (1). In contrast with most previous treatments,[1,2,4] we solve this equation after rewriting it in matrix form at the outset. By using basis kets $\{|m\rangle\}$ defined by $S_z|m\rangle = \hbar m|m\rangle$ $(m = -S, -S+1, \ldots S)$, ψ is written as

$$\psi = \sum_{m=-S}^{S} C_m(t)|m\rangle$$

and we have a coefficient vector $\mathbf{C}$ with mth component $C_m(t)$. $\mathbf{C}$ obeys the matrix equation

$$i\hbar\, d\mathbf{C}/dt = \tilde{H}\mathbf{C}. \tag{3}$$

$\tilde{H}$ is a $(2S+1)\times(2S+1)$ real-symmetric matrix:

$$\tilde{H} \equiv \tilde{H}_0 + \tilde{V}\sum_{n=-\infty}^{\infty}\delta(t-2\pi n)$$

with

$$(\tilde{H}_0)_{m,m'} = A\hbar^2 m^2 \delta_{m,m'}$$

and

$$(\tilde{V})_{m,m'} = -(\mu B/2)\hbar\{[\hat{S}^2 - m'(m'+1)]^{1/2}\delta_{m,m'+1} + [\hat{S}^2 - m'(m'-1)]^{1/2}\delta_{m,m'-1}\},$$

where $\hat{S} = [S(S+1)]^{1/2}$. Noting the periodicity $\tilde{H}(t+2\pi) = \tilde{H}(t)$, we apply Floquet's theorem: The solution of Eq. (3) just after the nth pulse is

$$\mathbf{C}(2\pi n + 0) = \sum_{\alpha}[\exp(-2\pi i n E_\alpha/\hbar)][\mathbf{X}_\alpha^\dagger \cdot \mathbf{C}(+0)]\mathbf{X}_\alpha,$$

where $\{E_\alpha\}$ and $\{\mathbf{X}_\alpha\}$ are the quasienergies and eigenstate vectors, respectively, obtained by solving the eigenvalue problem $\tilde{U}\mathbf{X}_\alpha = \exp(-2\pi i E_\alpha/\hbar)\mathbf{X}_\alpha$. ($\mathbf{X}_\alpha^\dagger$ is the Hermitian conjugate of $\mathbf{X}_\alpha$.) Here $\tilde{U}$ is a one-cycle unitary matrix defined in terms of the time-ordering operator T as follows:

$$\tilde{U} = T\exp\left[\int_{+0}^{2\pi+0}(-i/\hbar)\tilde{H}(t')dt'\right] = \exp[(-i/\hbar)\tilde{V}]\exp[(-i/\hbar)2\pi\tilde{H}_0]. \tag{4}$$

To make the numerical diagonalization of $\tilde{U}$ more tractable, we note the following points. First, because of the symmetry of Eq. (1) with respect to the reversal of the quantization axis ($S_z \to -S_z$), both Eqs. (3) and (4) can be decomposed into decoupled even- and odd-parity parts. Second, we take $\hbar = \hat{S}^{-1}$, i.e., $\mathbf{S}^2 = \hbar^2\hat{S}^2 = 1$ so that the observable magnitude $\mathbf{S}^2$ maintains its classical value. $\hbar$ is thereby irrational for any integer value of S, ensuring the pseudorandomness of matrix elements in Eq. (4).

We choose to describe quasienergy states

$$|\alpha\rangle = \sum_{m=-S}^{S}(\mathbf{X}_\alpha)_m|m\rangle$$

in terms of spin-coherent states (minimum-uncertainty states)[6]

$$|\theta,\phi\rangle = \exp[-i\theta(S_x\sin\phi - S_y\cos\phi)]|-S\rangle:$$

$$\langle\theta,\phi|\alpha\rangle = \sum_{m=-S}^{S}(\mathbf{X}_\alpha)_m\langle\theta,\phi|m\rangle.$$

The probability density function $P_\alpha(\theta,\phi) = |\langle\theta,\phi|\alpha\rangle|^2$ mimics classical orbits nicely. [For the state $|\pi/2,0\rangle$ (i.e., minimum uncertainty packet around $\theta=\pi/2$, $\phi=0$), this probability gives

$$P(\theta,\phi) = |\langle\theta,\phi|\pi/2,0\rangle|^2 = \cos^{4S}(\lambda/2)$$

with $\cos\lambda = \sin\theta\cos\phi$. For $S \gg 1$,

$$P(\theta,\phi) = [(1+\cos\lambda)/2]^{2S} \cong (1-(\theta-\pi/2)^2/4-\phi^2/4)^{2S} \simeq \exp[-S(\theta-\pi/2)^2/2]\exp(-S\phi^2/2),$$

which indicates a minimum linear scale of $O(\hat{S}^{-1/2})$ in the (θ,ϕ) plane.] Figures 2(a)–2(d) show mountainous profiles of $P_\alpha(\theta,\phi)$ for $S=128$. Figures 2(a) and 2(d) correspond typically to a classical KAM torus

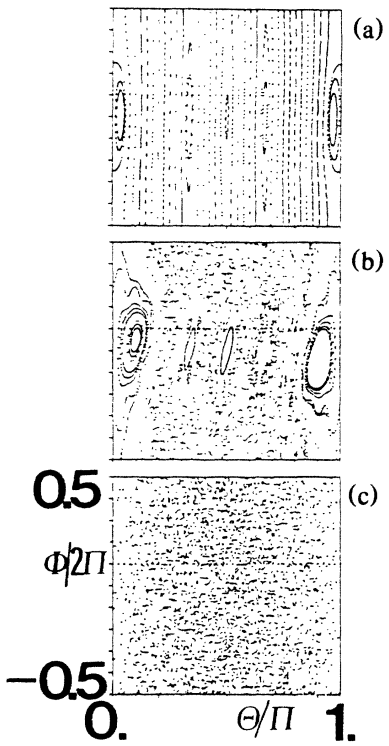

FIG. 1. Classical orbits in ϕ-θ plane ($0 \le \theta \le \pi$, $-\pi \le \phi \le \pi$). 41 orbits with initial values $\phi = 0.2$ and $\theta = j\pi/40$ ($j = 0, 1, \ldots, 40$) are shown: (a) $\mu B = 0.01$; (b) $\mu B = 0.20$; (c) $\mu B = 1.0$.

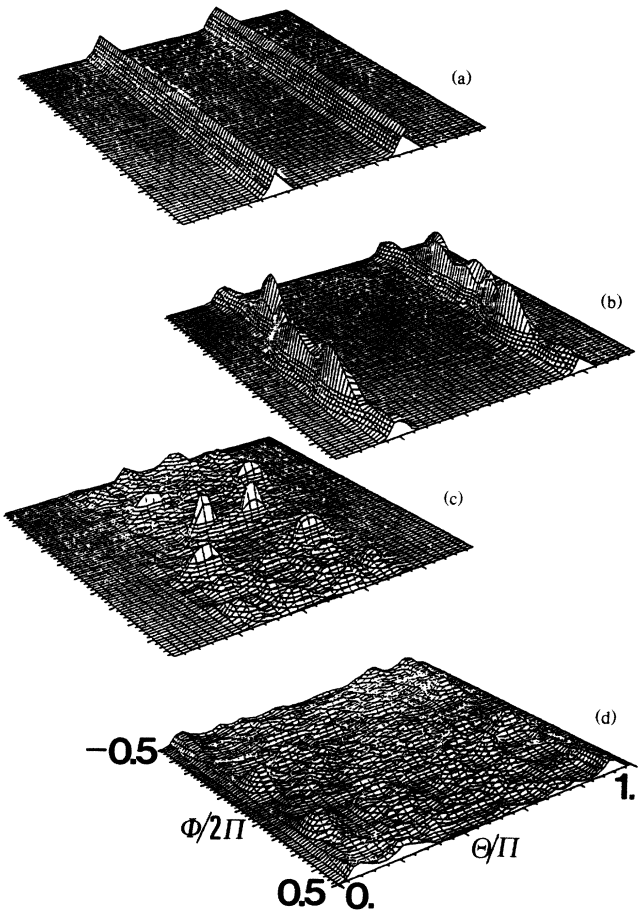

FIG. 2. Three-dimensional pictures of $P_\alpha(\theta,\phi)$ for $S=128$. (This spin magnitude is retained throughout in Figs. 2–5.) (a) $\mu B=0.01$, $E/\hbar=0.1439$; (b) $\mu B=0.20$, $E/\hbar=0.3849$; (c) $\mu B=0.20$, $E/\hbar=0.1296$; (d) $\mu B=1.0$, $E/\hbar=0.9006$.

for $\mu B \leq \mu B_1$ and global chaos for $\mu B \geq \mu B_2$, respectively. [Compare Figs. 1(a) and 1(c).] Figures 2(b) and 2(c) correspond to a deformed KAM torus and bounded chaos, respectively, in the region $\mu B_1 \leq \mu B \leq \mu B_2$ [compare Fig. 1(b)]. These results indicate closer examination of wave-function localization and structure. The contour map of $P_\alpha(\theta,\phi)$ is given in Fig. 3(a), where several contours are depicted for the chaotic pattern in Fig. 2(d). We clearly see tendrils or whorls with very fine structures, similar to fractal objects.

In an attempt to quantify $P_\alpha(\theta,\phi)$ in terms of fractals,[7] we define scale-dependent binary patterns by coarse graining of a projection of the three-dimensional structures $P_\alpha(\theta,\phi)$: For a linear scale ϵ, we consider the square $\epsilon\times\epsilon$ mesh $A(\epsilon)$ around the position (θ,ϕ) and assign $+1$ to it if the condition

$$\int_{(\theta,\phi)\subset A(\epsilon)} P_\alpha(\theta,\phi)\,d\Omega \Big/ \int_{(\theta,\phi)\subset A(\epsilon)} d\Omega \geq h_c$$

is satisfied, and -1 otherwise, where $d\Omega = \sin\theta\, d\theta\, d\phi$. For all meshes in the (θ,ϕ) plane, this procedure yields the two-dimensional binary phase pattern $(P_\alpha)_\epsilon$ on a resolution ϵ. The left-hand side of the above unequality is the average of P_α over surface elements of the unit radius sphere and h_c [$\equiv 4\pi\nu/(2S+1)$] is a scale-independent height with a con-

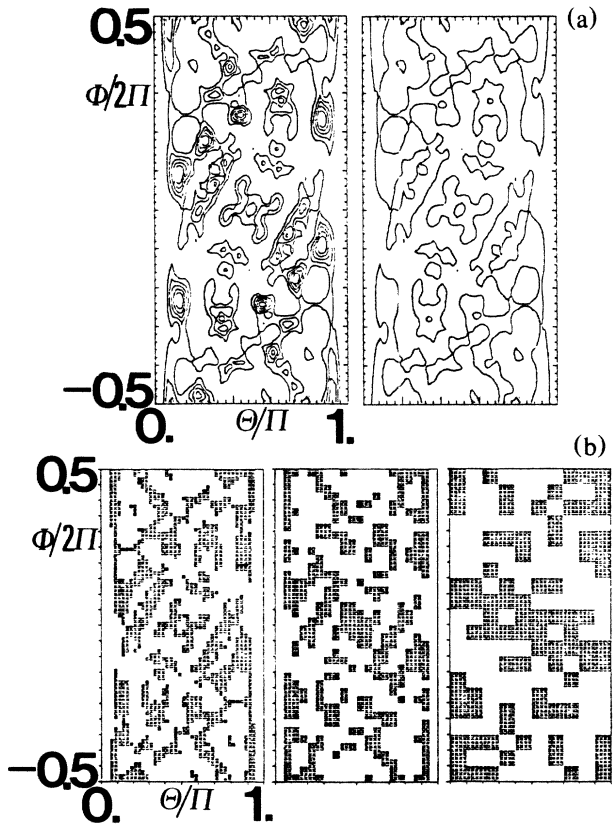

FIG. 3. Contour map for $P_\alpha(\theta,\phi)$ of Fig. 2(d): (a) Five contour levels with height $=0.004l$ ($l=1,2,\ldots,5$) (left-hand panel); single contour ($l=1$) level (right-hand panel). (b) Scale-dependent binary patterns $(P_\alpha)_\epsilon$ (from left, $\epsilon=\epsilon_0\rightarrow 2\epsilon_0\rightarrow 2^2\epsilon_0$). Black meshes are used for $+1$ phase. The height is $h_c=0.004$, i.e., $\nu=0.0818$. [This h_c value is used throughout in Figs. 3(b), 4, and 5.]

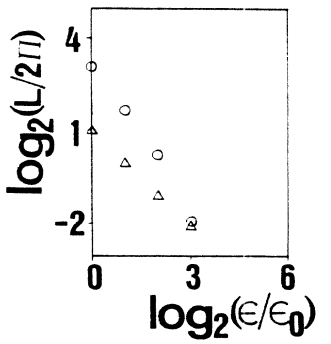

FIG. 4. ϵ dependence of perimeter length on logarithmic scales: triangles and circles correspond to Figs. 2(a) and 2(d), respectively.

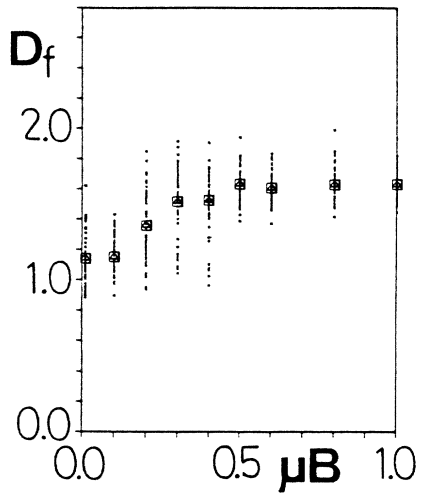

FIG. 5. Field-dependence of D_f distributions. The triangle-in-square symbol indicates the average value $\langle D_f \rangle$. D_f values are calculated by least-squares fits to data of Fig. 4.

venient fractional factor ν. ϵ is increased as $\epsilon = 2^{n-1}\epsilon_0$ ($n = 1, 2, \ldots$) with ϵ_0 the minimum scale of $O(\hbar^{1/2}) = O(\hat{S}^{-1/2})$. Both the nodal and vertical structures of $P_\alpha(\theta, \phi)$ are naturally captured by $(P_\alpha)_\epsilon$. Figure 3 (b) shows the variation of binary-phase patterns with increasing scales $\epsilon = \epsilon_0 \rightarrow 2\epsilon_0 \rightarrow 2^2\epsilon_0$ with $\epsilon_0 = \pi/40$, appropriate for $S = 128$. The most striking fractal feature appears in the drastic variation of perimeter lengths for phase-pattern boundaries as the grid scale ϵ is changed.[8] In Fig. 4, ϵ dependences of perimeter lengths L (Legesque measures) are shown for regular [Fig. 2(a)] and irregular [Fig. 2(d)] wave functions. They fit the scaling law $-d\ln L/d\ln\epsilon = D_f$, where D_f is a fractal dimension. We find $D_f = 1.0$ and 1.58 for wave functions related to KAM torus and chaos, respectively. We have calculated D_f for all of the even-parity quasienergy states. In Fig. 5, the distribution of D_f is shown for several values of μB. $\langle D_f \rangle$, i.e., average of D_f over quasienergies, shows plateaus for $\mu B \lesssim 0.1$ and $\mu B \gtrsim 0.5$, with $\langle D_f \rangle \cong 1.14$ and 1.62 in the former and latter regions, respectively. For $0.1 \lesssim \mu B \lesssim 0.5$, $\langle D_f \rangle$ increases with μB. Large fluctuations of D_f in this intermediate region reflect the coexistence of KAM tori and chaos in the classical limit. The critical values $\mu B \cong 0.1$, and 0.5 compare closely with μB_1 and μB_2, respectively, observed in the classical treatment. This finding strongly suggests that, in contrast with quantum kicked rotators,[1,2] the persistence of quantum diffusion, rather than its suppression, seems to be characteristic of the present spin system for large S. When the height h_c is varied by $\pm 20\%$, values D_f show little change in classically regular regimes but definite changes in chaotic regimes. Nevertheless, the general trend above is found to be unaltered.

In conclusion, the spin-coherent state representation of wave functions in a pulsed spin system shows quasifractal patterns in semiclassically large-spin regions, whose scale-dependent contours have perimeters characterized by a fractal dimension D_f. Variation of D_f with increasing magnetic field clearly coincides with the transition from predominantly KAM tori to global chaos in the classical dynamics.

One of authors (K.N.) acknowledges valuable discussions with H. J. Mikeska, C. Jeffries, and K. Kawasaki. He thanks the Theoretical Division, Los Alamos National Laboratory, and the Department of Physics, University of California, Berkeley, for their hospitality.

[a]Present address: Central Research Laboratories, Sumitomo Metal Industries, Ltd., Amagasaki 660, Japan.

[1]G. Casati, B. V. Chirikov, F. M. Izrailev, and J. Ford, in *Stochastic Behavior in Classical and Quantum Hamiltonian Systems*, edited by G. Casati and J. Ford (Springer, Berlin, 1979); T. Hogg and B. A. Huberman, Phys. Rev. Lett. **48**, 711 (1982); S. Fishman, D. R. Grempel, and R. E. Prange, Phys. Rev. Lett. **49**, 509 (1982).

[2]H. J. Korsch and M. V. Berry, Physica (Amsterdam) **3D** 627 (1981); D. L. Shepelyansky, Dokl. Akad. Nauk. SSSR **256**, 586 (1981) [Sov. Phys. Dokl. **26**, 80 (1981)].

[3]K. Nakamura, S. Ohta, and K. Kawasaki, J. Phys. C **15**, L143 (1982); S. Ohta and K. Nakamura, J. Phys. C **16**, L605 (1983); G. Gibson and C. Jeffries, Phys. Rev. A **29**, 811 (1984); X. Zhang and H. Suhl, Phys. Rev. A **32**, 2530 (1985); F. M. de Aguiar and S. M. Rezende, Phys. Rev. Lett. **56**, 1070 (1986).

[4]F. Hakke, M. Kus, J. Mostowski, and R. Scharf, to be published; H. Frahm and H. J. Mikeska, to be published. Quasirecurrent behaviors of the expectation value of **S** and quasienergy-level statistics were studied by the former and latter groups, respectively.

[5]In a specific limit $\mu B << 1 << A$, **S** is almost confined to the basal plane ($\theta = \pi/2$). Then, noting $4\pi A S_{nz} << \phi_n$, our combined map is reduced to the standard map [B. V. Chirikov, Phys. Rep. **52**, 263 (1979); J. M. Greene *et al.*, Physica (Amsterdam) **3D**, 468 (1981)] for action $\tilde{I}_n = 2AS_{nz}$ and angle $\tilde{\phi}_n = \phi_n/2\pi$ with a stochasticity parameter $k = 4\pi A \mu B$.

[6]J. M. Radcliffe, J. Phys. A **4**, 313 (1971). For the recent status, see, e.g., J. R. Klauder and B. Skagerstam, *Coherent States* (World Scientific, Singapore, 1985). Note also the recent application of Glauber coherent states [S. Chang and K. Shi, Phys. Rev. Lett. **55**, 269 (1985)] as coarse-grained Wigner functions.

[7]B. B. Mandelbrot, *The Fractal Geometry of Nature* (Freeman, New York, 1983).

[8]We have not investigated possible "fat fractal" area scaling because of insufficient grid scales; cf. K. Nakamura *et al.*, to be published.